Article

J. Mex. Chem. Soc. **2025**, *69*(4)
Regular Issue
©2025, Sociedad Química de México
ISSN-e 2594-0317

Excellent Catalytic Performance of Co_3O_4/CuO Nanocomposite for Catalytic Reduction of Nitroaromatic Compounds and Dyes Pollutants

Amir Hossein Sepahvand, Zohreh Derikvand*, Saeid Menati

Department of Chemistry, Khor.C., Islamic Azad University, Khorramabad, Iran.

***Corresponding author:** Zohreh Derikvand**,** e-mail: zderik@yahoo.com; zo.derik@iau.ac.ir

Received July 29th, 2024; Accepted January 7th, 2025.

DOI: http://dx.doi.org/10.29356/jmcs.v69i4.2340

Abstract. The paper investigates the catalytic reduction of nitroaromatic compounds (4-nitroaniline (4-NA) and 2-nitroaniline (2-NA)) by Co_3O_4/CuO nanocomposite. Also, the degradative property of nanocomposite was assessed using both anionic (methyl orange (MO)) and cationic (safranin O (SO)) dyes pollutants and simulated by the linear isotherm models and kinetic equations. Nano metal oxides CuO and Co_3O_4, as well as its nanocomposite, were synthesized using a precipitation-calcination method. The crystalline pattern, morphological structure, functionality, surface chemistry, and elemental content were evaluated. The catalytic efficiency in the reduction of nitroanilines and dyes was evaluated by sodium borohydride ($NaBH_4$). 100 % conversion of nitroanilines to their corresponding amines could be achieved in just 2 minutes for 4-nitroaniline and 10 minutes for 2-nitroaniline. The Co_3O_4/CuO nanocomposite shows 100 % and 76.6 % TOC for degradation of MO and SO. Additionally, the nanocomposite demonstrated stable performance over five consecutive reduction cycles for both dyes and NAs. Overall, the synthesized Co_3O_4/CuO nanocatalyst proves to be a cost-effective and high-performing candidate for remediation of pollutants in wastewater. Its easy recovery nature and efficient catalytic performance make it an excellent choice for environmental cleanup efforts.
Keywords: 4-Nitroaniline; Co_3O_4/CuO; safranin O; methyl orange; catalytic reduction.

Resumen. El artículo investiga la reducción catalítica de compuestos nitroaromáticos (4-nitroanilina (4-NA) y 2-nitroanilina (2-NA)) mediante un nanocompuesto de Co_3O_3/CuO. Además, se evaluó la propiedad degradativa del nanocompuesto utilizando colorantes contaminantes aniónicos (naranja de metilo (MO)) y catiónicos (safranina O (SO_3)) y se simuló mediante modelos de isotermas lineales y ecuaciones cinéticas. Los nanoóxidos metálicos CuO y Co_3O_3, así como su nanocompósito, se sintetizaron mediante un método de precipitación-calcinación. Se evaluaron el patrón cristalino, la estructura morfológica, la funcionalidad, la química superficial y el contenido elemental. La eficiencia catalítica en la reducción de nitroanilinas y colorantes se evaluó mediante borohidruro de sodio ($NaBH_3$). La conversión del 100 % de nitroanilinas a sus aminas correspondientes se logró en tan solo 2 minutos para la 4-nitroanilina y 10 minutos para la 2-nitroanilina. El nanocompuesto de Co_3O_3/CuO muestra un 100 % y un 76,6 % de COT para la degradación de MO y SO. Además, el nanocompuesto demostró un rendimiento estable durante cinco ciclos de reducción consecutivos tanto para colorantes como para NA. En general, el nanocatalizador de Co_3O_3/CuO sintetizado demuestra ser un candidato rentable y de alto rendimiento para la remediación de contaminantes en aguas residuales. Su fácil recuperación y su eficiente rendimiento catalítico lo convierten en una excelente opción para las iniciativas de limpieza ambiental.
Palabras clave: 4-Nitroanilina; Co_3O_3/CuO; safranina O; naranja de metilo; reducción catalítica.

J. Mex. Chem. Soc. **2025**, *69*(4)
Regular Issue
©2025, Sociedad Química de México
ISSN-e 2594-0317

Introduction

N Nitroanilines (NAs) are commonly utilized in the fabrication of fuel additives, insecticides, pharmaceuticals, dyestuffs and plastics [1-4]. Among them, 4-nitroaniline (4-NA) is an especially hazardous chemical that poses serious environmental risks, including mutagenic and teratogenic effects [5,6]. This dangerous compound is often found in wastewater from industries involved in pesticide manufacturing, dyeing, petrochemicals, oil refining, and chemical paints [7-9]. Due to its high solubility, 4-NA can easily infiltrate water and soil, leading to environmental contamination [9]. In some regions, sewage sludge is commonly recycled and used as fertilizer in agricultural fields [10]. However, the presence of toxic compounds such as chloroaniline and nitroaniline in sewage sludge can be detrimental to the environment [11]. The Environmental Protection Agency (EPA) has categorized 4-NA as a priority pollutant, with levels recorded in the environment reaching up to 100 mg L^{-1} [8]. The presence of 4-nitroaniline (4-NA) in water is a serious concern for both developed and developing countries due to its harmful effects on human and aquatic life [8]. As a high-priority water contaminant, there are strict regulations on the manufacturing, use, and disposal of 4-NA [12]. It is imperative to find sustainable and environmentally friendly methods for removing 4-NA pollution. Numerous methods have been employed to detect and remove 4-NA using various materials. The use of nanomaterials in developing new catalyst platforms has emerged as a promising alternative to traditional methods. Recent research has highlighted the unique characteristics and applications of nanomaterials in addressing 4-NA contamination in water [13]. Bimetallic oxides have garnered considerable attention due to their unique properties that differ from those of monometallic components [14,15]. It is widely recognized that incorporating a second metallic component can improve the selectivity, activity and stability of pure metal catalysts [16,17]. The urgent need to remove 4-nitroaniline (4-NA) from the environment is undeniable, prompting the exploration of various technologies to address this challenge. Despite the use of technologies such as thermal degradation, electrocoagulation, adsorption, ozonation, photodegradation, electrochemical degradation, electro-Fenton method, and biodegradation [18-24], these methods often face drawbacks such as generation of secondary pollutants, prolonged treatment times, low efficiency, adverse environmental impacts and high costs [25-28]. This has led to the search for alternative methods [29], among which catalytic reduction via $NaBH_4$ has emerged as a promising and environmentally friendly approach to converting nitroaniline to aminoaniline [30-31]. The reduction reaction is of significant interest due to the production of 4-aminoaniline, an intermediate with various industrial applications in engineering polymer, hair dyes, rubber antioxidant and hena. Catalytic reduction reactions rely heavily on the choice of catalyst, emphasizing the importance of developing efficient catalysts with robust adsorption capacity for $NaBH_4$, stability, affordability, and excellent electron transfer capabilities. This not only benefits industrial and economic aspects but also plays a crucial role in achieving environmental goals.

The presence of toxic dyes, which pose serious risks to both aquatic ecosystems and human health, is a significant environmental concern that leads to the depletion of aquatic life [32]. Some of the detrimental effects include respiratory issues, skin cancer, pneumonia, genetic disorders, and cardiovascular diseases. [33]. To address the challenges posed by toxic dyes in water, various technologies and processes have been developed to effectively remove these contaminants from wastewater. These methods encompass physical, chemical, and biological approaches [34]. Catalytic reactions are particularly important in this context, as they can function under mild conditions, thereby lowering the costs and energy requirements of the treatment process while maintaining high selectivity [35].

This study focused on the synthesis and application of Co_3O_4/CuO nanocomposite for the reduction of dye pollutants and nitroanilines with $NaBH_4$ as a reductant. The results clearly show the effectiveness of the nanocomposite in reducing all mentioned contaminants. A key benefit of this nanocatalyst is its easy recyclability and reusability, making it cost-effective for practical use. Additionally, the nanocomposite is easy to synthesize, highly stable, exhibits strong catalytic activity, aligns with green chemistry principles, and can operate under mild reaction conditions. It is worth mentioning that all experiments were conducted using water as a solvent, known for being the most environmentally friendly option due to its low impact, safety, affordability, and eco-friendliness.

J. Mex. Chem. Soc. **2025**, *69*(4)
Regular Issue
©2025, Sociedad Química de México
ISSN-e 2594-0317

Experimental

Preparation of Co_3O_4/CuO nanocatalyst

To synthesize the Co_3O_4/CuO nanocomposite, a well-defined procedure was followed. Initially, an aqueous solution containing cobalt (III) nitrate hexahydrate and copper (II) nitrate trihydrate in a 3:4 molar ratio in 20 mL of distilled water was prepared. The reaction mixture was stirred until a clear solution was obtained. Subsequently, the pH of reaction mixture was carefully adjusted to 9 using ammonium solution (3M). The obtained solid product was sonicated for 1 hour. The resulting product was filtered, washed with deionized water and ethanol several times, and dried at 80 °C for 24 hours. The Co_3O_4/CuO nanocomposite was obtained by calcined precursor at 700 °C in air for 5 hours. Similar experiments have been done for preparation of CuO and Co_3O_4 nanoparticles.

Characterization of catalyst

The Fourier transform infrared (FT-IR) spectra were taken by means of a Perkin-Elmer Spectrum RXI FT-IR spectrophotometer in the range of 4000-400 cm^{-1}. Powder X-ray diffraction (XRD) analyses were performed with a Ni-filtered Cu Kα radiation X-ray diffractometer (PANalytical/X'Pert Pro MPD) with a wavelength (λ) of 1.5406 Å. UV-vis spectra were obtained through a Perkin-Elmer Lambda 25 UV-vis spectrophotometer, covering the wavelength range of 200–600 nm. An in-depth investigation into the size and morphology of the Co_3O_4/CuO nanocomposite was conducted using a MIRA3 TESCAN field emission scanning electron microscope (FESEM) equipped with an energy dispersive X-ray (EDX) analyzer. The surface area of the nanocomposite was determined using the Brunauer Emmett Teller (BET) model. This involved N_2 gas adsorption–desorption isotherm measurements conducted on a BELSORP Mini II instrument. Furthermore, the Barrett-Joyner-Halenda (BJH) method was utilized to study the pore size and volume pore distribution of the nanocomposite.

Catalytic activities test for the reduction of nitroanilines and dyes

The catalytic activity of the CuO, Co_3O_4 and Co_3O_4/CuO nanocomposite in the reduction of nitroanilines and dyes (MO and SO) with an excess of $NaBH_4$ was methodically evaluated in a quartz cell at indoor temperature. The catalytic reduction of 2-nitroaniline (2-NA) by $NaBH_4$ served as the model reaction, and the reaction progress was monitored via UV-vis spectroscopy. For the catalytic assessment, a quartz cell containing 2 mL of 2-NA (0.2 mM) was utilized. To this, 0.5 mL of $NaBH_4$ (20 mM) was added, followed by the introduction of a proper amount of the catalyst. Subsequently, at 2-minute intervals, the conversion of 2-NA was scrutinized within the scanning range of 200-500 nm. Upon completion of the reaction, the catalyst was separated from the solution, subjected to multiple washes with deionized water (DI-H_2O), and then dried for subsequent cycles. The dosage of catalyst for the reduction reaction was investigated from 1 to 5 mg of catalyst, and the best amount of catalyst was 3 mg and the other experiment was done with 3 mg of catalyst. The degradation of methyl orange and safranin O (0.2 mM) was assessed in a quartz cell consisting of 2 mL of dye and 0.5 mL fresh $NaBH_4$ (20 mM). The progress of dyes reduction by Co_3O_4/CuO nanocomposite in the present and absence of $NaBH_4$ and desired amount of catalyst was monitored via UV-vis in the range of 200-700 nm.

Equations (1) and (2) were employed to calculate the rate constant and conversion efficiency. Also, the total conversion of dyes (TOC) was calculated by equations (2). C_0 and C_t represent the initial and time-dependent concentrations of nitroanilines or dyes, as determined by the absorption spectrum.

$$K_t = - \ln\frac{C_t}{C_0} \quad (1)$$

$$R(\%) = \frac{C_0 - C_t}{C_0} \times 100 \quad (2)$$

It's important to highlight that the pH of the solution created by mixing the dyes with $NaBH_4$ was initially measured at about 6.5 before the nanocomposite was added. A pH level below 7.0 is generally more conducive to the degradation process and has been shown to enhance catalytic activity. Therefore, no modifications to the pH were necessary, eliminating the need for any adjustments during the experiment.

J. Mex. Chem. Soc. **2025**, *69*(4)
Regular Issue
©2025, Sociedad Química de México
ISSN-e 2594-0317

Optimization of the synthesis conditions

In this study the impact of various factors such as amount of catalyst, concentration of dyes and nitroanilines were investigated for catalytic reduction reaction. Also, we evaluated the effect of molar ratio, temperature, pH and aging time on the production of Co_3O_4/CuO nanocomposite to determine the most positive synthesis conditions. Moreover, the concentration of $NaBH_4$ in the catalytic experiments underwent assessment. The results show that the best condition for preparation a pure nanocomposite obtain at pH=9 and calcinations at 700 °C. Consequently, it was observed that lower temperatures are insufficient for the production of Co_3O_4/CuO nanocomposite, leading in a multi-phase structure.

Results and discussion

Characterization of pure samples and Co_3O_4/CuO nanocomposite

The FT-IR spectrum of the pure samples and Co_3O_4/CuO nanocomposite was recorded at the 400-4000 cm^{-1} range to distinguish the functional groups and chemical bonds present in the samples (Fig. 1). The absorption bands at 536 cm^{-1} and 584 cm^{-1} are related to the Cu–O stretching vibrations of CuO nanoparticles in the monoclinic system. The bands appear at 700-500 cm^{-1} are assigned to metal oxides in nanocomposite. The stretching band for T_d system in Co_3O_4 are discernible at 725 cm^{-1} and 532 cm^{-1}, respectively [36]. A strong band at 1630 cm^{-1} corresponds to the OH vibration of water molecules that physically adsorbed on the surface of nanocomposite [37].The stretching vibrations in the range of 3000–3500 cm^{-1} are associated with the –OH groups of water molecules [37]. These FT-IR spectral features provide important insights into the chemical composition and functional groups present in the synthesized samples.

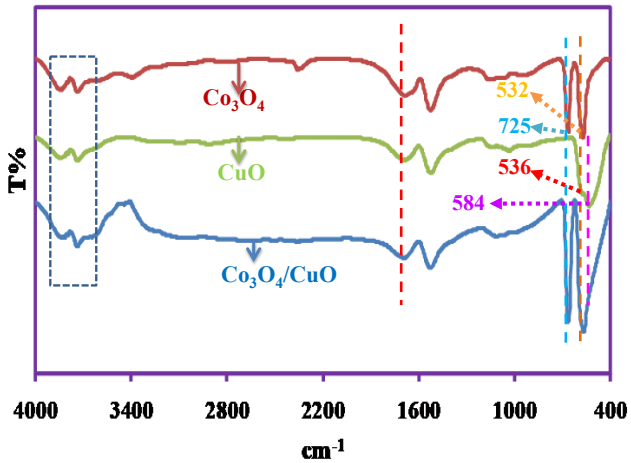

Fig.1. FT-IR spectra of Co_3O_4, CuO and Co_3O_4/CuO nanocomposite.

The XRD diffraction patterns of Co_3O_4/CuO nanocomposite, CuO and Co_3O_4 nanoparticles are illustrated in Fig. 2. Strong diffraction peaks located at 2θ =19.07 °, 31.33 °, 36.91 °, 44.88 °, 59.41 ° and 65.29 °, corresponding to (220), (311), (511), and (440) correspond to the (111), (220), (311), (400), (511) and (440) crystal planes of Co_3O_4 phases in accordance with the JCPDS card number 71–0816 [33]. Additionally, the peaks at 2θ =32.65 °, 35.68 °, 38.85 °, 48.91 °, 53.59 °, 61.67 °, 66.37 ° and 68.18 ° corresponding to various crystallographic planes, including (110), (002), (111), (202), (020), (113), (311), and (220), which are indicative of copper oxide, in accordance with the JCPDS card number 45-1548. The peaks of CuO were determined to be pure copper oxide, and the diffraction peaks of the samples were sharp, which indicates that the CuO is monoclinic. As depicted in Fig. 2, the Co_3O_4/CuO nanocomposite exhibits the coexistence of CuO and Co_3O_4 phases without any impurity phase.

J. Mex. Chem. Soc. **2025**, *69*(4)
Regular Issue
©2025, Sociedad Química de México
ISSN-e 2594-0317

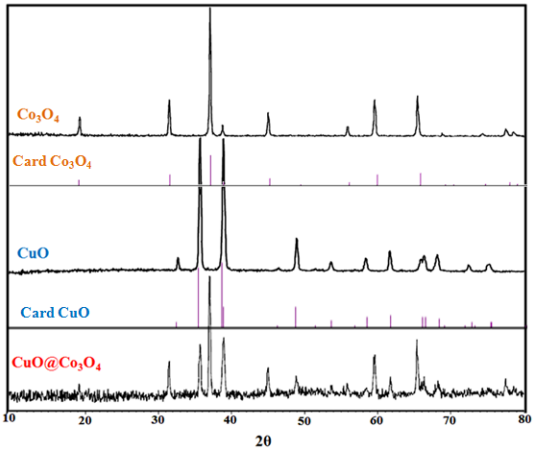

Fig. 2. XRD pattern of CuO, Co_3O_4 and Co_3O_4/ CuO nanocomposite.

The results of SEM analysis are shown in Fig. 3, revealing the shape, size and surface morphology, of the prepared structures. The SEM images in Fig. 3 demonstrate that the nanocomposite comprises nanohexagonal persmatic. The particle sizes are uniform with average diameter of about 57-59 nm. The particle sizes for CuO and Co_3O_4 are about 38-40 nm and 55-57 nm respectively. To further investigate the elemental distribution and composition of the Co_3O_4/CuO nanocomposite, EDX mapping measurements were conducted (Fig. 4). The EDX analysis shows the existence of Cu, Co, and O elements with atomic percentages of 18.76, 29.56, and 51.68 respectively. Indeed, these obtained atomic percentages are in well agreement with the prepared Co_3O_4/CuO nanocomposite. It can been seen from the maps in Fig.4 all elements are uniformly distributed over the samples, validating the homogeneity of the nanocomposites. Fig. 5 presents the N_2 adsorption-desorption isotherm curves for the synthesized Co_3O_4/CuO nanocomposite, which exhibits a type IV isotherm along with an H_3 hysteresis loop in the relative pressure range of P/P_0 = 0.4-1. This behavior indicates the presence of a porous structure. The effective BET specific surface areas of the synthesized nanoparticles were measured to be 4.59 m^2/g for the Co_3O_4/CuO nanocomposite, 4.19 m^2/g for Co_3O_4, and 4.10 m^2/g for CuO. Notably, the adsorption capacity of the Co_3O_4/CuO nanocomposite significantly increased at a relative pressure of P/P_0<0.4. This enhancement can be attributed to the nanocomposite's specific surface area, which promotes monolayer adsorption of N_2 onto the walls of its mesoporous structure. Additionally, using the BJH method applied to the adsorption branch of the N_2 isotherm, the average pore diameter was calculated to be 2 nm, with a total pore volume of 0.014 cm^3/g for the Co_3O_4/CuO nanocomposite.

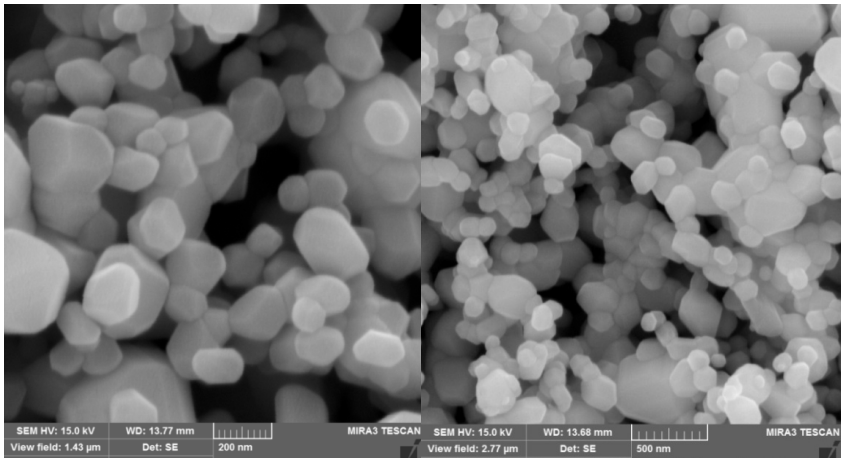

Fig. 3. SEM images of Co_3O_4/CuO nanocomposite.

J. Mex. Chem. Soc. **2025**, *69*(4)
Regular Issue
©2025, Sociedad Química de México
ISSN-e 2594-0317

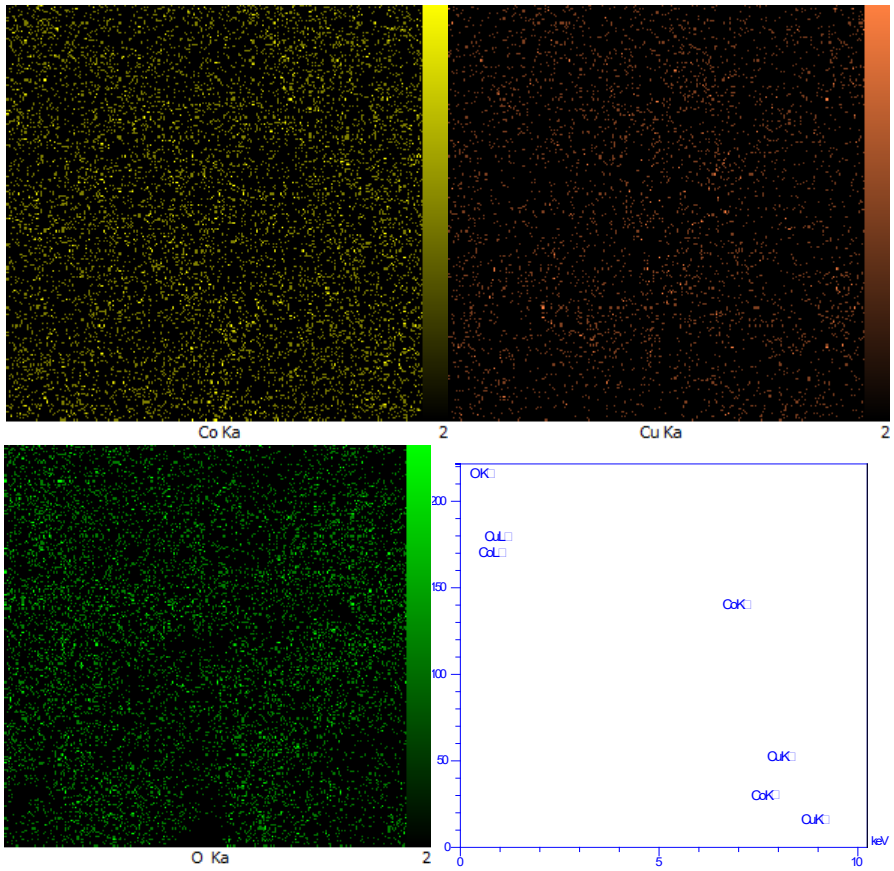

Fig.4. EDX diagrams and the corresponding elemental mapping images of Co_3O_4/CuO nanocomposite.

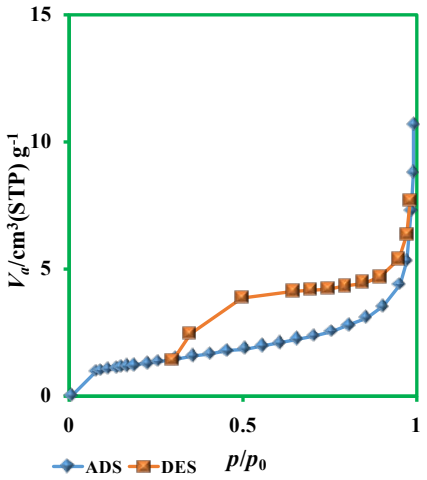

Fig.5. N_2 desorption-desorption isotherm of Co_3O_4/CuO nanocomposite.

J. Mex. Chem. Soc. **2025**, *69*(4)
Regular Issue
©2025, Sociedad Química de México
ISSN-e 2594-0317

Catalytic reduction of nitroanilines

The as prepared Co_3O_4, CuO and Co_3O_4/CuO samples used as catalyst for the reduction of nitroanilines, in the presence of $NaBH_4$ as a reducing agent. Initially, we used 2-nitroaniline to optimum the reaction condition and the progress of reduction reaction was monitored by UV–vis spectroscopy. Normally, 2-nitroaniline solution shows a broad peak around 412 nm [31]. Upon adding $NaBH_4$ to the reaction mixture, the intensity of this peak remains unchanged after 30 minutes validating that the reduction reaction has not occurred without a catalyst due to a high kinetic barrier between the donor and acceptor molecules (BH_4^- and 2-NA, respectively). As a result, the addition of a catalyst to the reaction mixture is essential to conquer this kinetic barrier, providing the monitoring of the reduction reaction by UV–vis spectroscopy. To explore this, parallel experiments were carried out by the 2-NA-$NaBH_4$-catalyst solution. With adding catalyst into the reaction mixture, the intensity peak at 412 nm starts to reduce. The reduction reaction of 2-NA was completed within 18 minutes and 30 minutes in the presence of CuO and Co_3O_4**,** respectively (Fig. 6**(a)** and **(b)**). However the reduction reaction was completed after 10 minutes with Co_3O_4/CuO nanocomposite (Fig. 6**(c)**). Outstandingly, with the reduction reaction completion a clear, colorless solution was obtained. Based on the obtained results the Co_3O_4/CuO nanocomposite illustrates excellent activity toward 2-nitroaniline reduction into its corresponding 2-aminaniline (2-AA). For finding the best amount of catalyst some experiments were performed with 1mg to 5 mg catalyst and the best performance was observed for 3 mg of catalyst in the presence of 2−NA−$NaBH_4$−H_2O solution. The results show a distinguished acceleration in the rate of reduction reaction with increasing dosage of Co_3O_4/CuO nanocatalyst, carrying out the reaction below 1 minute and it was hard to monitor the progress of reaction in appropriate time. Therefore, we chose 3mg of catalyst as the optimal quantity for subsequent experiments with Co_3O_4/CuO nanocatalyst. The increase of Co_3O_4/CuO nanocatalyst dosage facilitates better accessibility to active sites for 2-NA adsorption, thus enhancing the reduction reaction rate. The better catalytic efficiency of the Co_3O_4/CuO nanocomposite can be attributed to the close contact between Co_3O_4 and CuO, which facilitates electron transfer from BH_4^- to 2-NA. The synergistic effect of Co_3O_4 and CuO into the nanocomposite raises the accessibility of active sites for the production of H_2 and e^- (from $NaBH_4$) on the Co_3O_4/CuO surface, accordingly accelerating the reduction reaction speed. At first, H_2 molecules are generated by the reaction of water and BH_4^- ions. Then, these molecules and 2-nitroaniline are adsorbed simultaneously onto the surface of the Co_3O_4/CuO nanocomposite. The nanoparticles in the Co_3O_4/CuO nanocomposite facilitate electron transfer to 2-NA, effectively overcoming the reaction kinetic barrier. After that adsorbed BH_4^- ions, released hydrogen as hydride, the hydride anion transfers to the metal in the Co_3O_4/CuO nanocomposite and producing a complex. Eventually, the nitro group of the 2-nitroaniline is reduced by taking the hydride from the complex. Subsequent to three hydro-deoxygenation reactions, 2-AA is formed. In the final step, 2-AA is desorbed from the nanocomposite's surface. The Langmuir-Hinshelwood model was applied to estimate the performance of the Co_3O_4/CuO nanocomposite for kinetic analysis. Since the concentration of $NaBH_4$ solution was high relative to 2-NA concentration, the pseudo-first-order kinetics model was considered to determine the reaction rate constants (k). The kinetics were investigated using the equation $\ln(C_t/C_0) = -kt$, where C_0 and C_t correspond to the first and time 't' concentrations of 2-nitroaniline, respectively [29-31]. Fig. 6**(d)** illustrates a linear relationship between $\ln(C_t/C_0)$ and time during the reduction reaction catalyzed by Co_3O_4/CuO nanocomposite, validating the pseudo-first-order kinetics. The rate constant (k) was determined from the slope of the straight line, yielding a value about 0.408 min^{-1} for the Co_3O_4/CuO nanocatalyst, indicating excellent performance in converting 2-NA to 2-AA. This excellent catalytic efficiency is related to the close contact and interaction between Co_3O_4 and CuO nanoparticles. The results of this study on reducing 2-nitroaniline using the 2-NA-$NaBH_4$-H_2O system was compared with other studies, as illustrated in Table 1 [31,36-40]. Here we compared different parameters with other reported previously for reducing 2-nitroaniline to 2-aminoaniline (Table 1). The Co_3O_4/CuO nanocomposite exhibited exceptional catalytic activity in reducing 2-nitroaniline (Table 1). The dosage of the catalyst in our study was lower compared to those given in Table 1. Additionally, the concentration of 2-nitroaniline in our study was higher than in previous reports. The Co_3O_4/CuO nanocatalyst used in this study was constructed without toxic or expensive materials, making it suitable for practical applications. Furthermore, the prepared Co_3O_4/CuO nanocomposite displayed astonishing efficacy in reducing 4-nitroaniline (4-NA) with $NaBH_4$, as shown in Fig. 6**(e)**. The data clearly indicate a significant decrease in the characteristic absorption peak of 4-nitroaniline (4-NA) at 374 nm, which is accompanied by the emergence of two new peaks at 239 nm and 305 nm. These new peaks correspond to the characteristic absorption of 4-aminoaniline (4-AA). As shown in Fig. 6**(e)**, the addition of the Co_3O_4/CuO nanocomposite resulted in a notable reduction in UV-vis absorption at 374 nm, while the absorption at 305 nm

J. Mex. Chem. Soc. **2025**, *69*(4)
Regular Issue
©2025, Sociedad Química de México
ISSN-e 2594-0317

increased. This change reflects a decrease in the concentration of 4-NA and a corresponding increase in the concentration of 4-AA at 305 nm. The reduction reaction was completed within just 2 minutes. To study the stability and reusability of Co_3O_4/CuO nanocomposite, the used catalyst was collected, washed with H_2O/EtOH several times and dried to use for new runs. Based on the results, the catalytic activity remained unchanged after four runs. These findings confirm the stability and excellent catalytic efeciency of the Co_3O_4/CuO nanocomposite compared to the fresh catalyst. As a result, the Co_3O_4/CuO nanocomposite appears as an excellent, efficient, stable, and reusable catalyst for the reduction of nitroanilines and other nitroaromatic compounds.

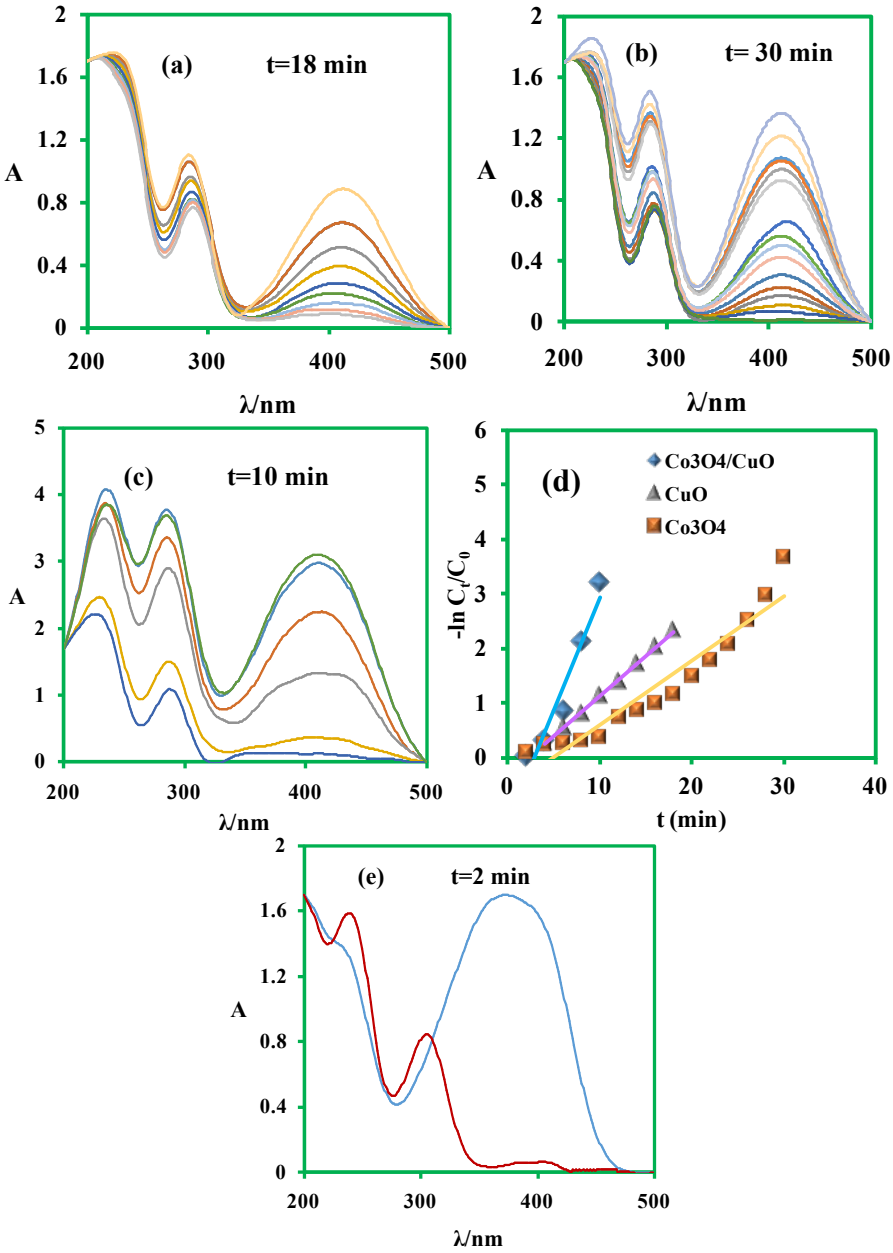

Fig. 6. The reduction of 2-nitroaniline (2-NA) in the presence of **(a)** CuO, **(b)** Co_3O_4, **(c)** Co_3O_4/CuO with $NaBH_4$ and 3 mg of catalysts **(d)** plot illustrating pseudo-first order kinitic, $\ln(C_t/C_0)$ verses reaction time (k = 0.147 min^{-1} (CuO), k = 0.117 min^{-1} (Co_3O_4), k = 0.408 min^{-1} (Co_3O_4/ CuO), **(e)** The reduction of 4-nitroaniline (4-NA) in the presence of Co_3O_4/CuO nanocomposite.

J. Mex. Chem. Soc. **2025**, *69*(4)
Regular Issue
©2025, Sociedad Química de México
ISSN-e 2594-0317

Table 1. Comparative characteristics of catalysts for reducing 2-nitroaniline.

Entry	Catalyst	$NaBH_4$ conc.	Catalytic activity (%)	Catalyst amount	2-NA conc.	Time (min)	Ref.
1	$CoFe_2O_4$/ZrMCM4125%	20 mM	100%	5mg	0.2 mM ($k=0.15\ min^{-1}$)	12	[31]
2	Ag_3PO_4/PPy/PANI	10 mM	100%	1 mg	1 mM ($k=0.022 min^{-1}$)	120	[34]
3	$Cu_2O/TiO_2/Ti_3C_2$	10 mM	100%	10 mg	5mM ($K=0.163 min^{-1}$)	15	[35]
4	NiO NPs	14 mM	62%	5 mg	0.15 mM ($k=0.007\ min^{-1}$)	120	[36]
5	Co_3O_4/CuO	20 mM	100%	3 mg	0.2 mM ($0.408\ min^{-1}$)	10	This work

Reduction of safranin O and methyl orange by Co_3O_4/CuO

The degradation of carcinogenic anionic and cationic dyes, such as safranin O (SO) and methyl orange (MO) were investigated using $NaBH_4$ as a green reductant. The main aim was to evaluate the catalytic performance of Co_3O_4/CuO in the degradation of these dyes pollutants. Some experiments were carried out with SO and MO, and their results are exhibited in Figs. 7**(a)** and **(b)**. The results show that the peak intensity of SO and MO start to decrease when Co_3O_4/CuO nanocomposite and $NaBH_4$ solution added to the reaction mixture. In UV-vis spectrum MO show absorption peak at 482 nm assigned to the azo bond [41] and this absorption peak was monitored to follow the reduction reaction. As shown in Fig. 7**(a)** the peak at 482 nm disappeared after 4 minutes with 100 % TOC (total conversion). The first-order kinetic model depicting the reduction of MO is illustrated in Fig. 7**(c)**, showing the efficient catalytic behavior. In the absence of nanocatalyst the reduction reaction was not progressed. The calculated rate constant for MO is about 1.57 min^{-1} as shown in Fig. 7**(c)**. Table 2 compares the prepared Co_3O_4/CuO nanocomposite and others reported in the literature [42-44]. The spectrum of SO demonstrated a absorption peak at 507 nm [45] and it was selected to monitor the influence of the Co_3O_4/CuO nanocatalyst. The results show that, the absorption spectra of SO remain constant after one-hour reaction period, suggesting that decolorization did not happen in the absence of the catalyst. Furthermore, comparable outcomes were found in the case where only $NaBH_4$ was used. Upon adding Co_3O_4/CuO and $NaBH_4$ into the reaction mixture, the degradation profile of SO undergoes a gradual change, with approximately 76.6% degradation observed within 12 minutes, the degradation reaction was stopped after 12 minutes (Fig. 7**(b)**). These results emphasize the excellent catalytic ability of Co_3O_4/CuO nanocatalyst in the reduction of SO and MO with $NaBH_4$, confirming the vital role played by the nanocomposite due to its excellent catalytic activity. The first-order kinetic model of SO reduction in the presence of Co_3O_4/CuO is shown in Fig.7**(c)**. The Langmuir-Hinshelwood mechanism [46] accurately elucidates the degradation process of MO and SO dyes. In this mechanism, the dyes and BH_4^- ions undergo adsorption onto the surface of the Co_3O_4/CuO catalyst. The Co_3O_4/CuO catalyst facilitates transmit of electrons from BH_4^- ions to dyes. The Co_3O_4/CuO reduces the energy obstacle between the product and reactant, resulted in the achievement of the degradation reaction within 12 and 4 minutes for SO and MO, respectively [47]. The percentage of degradation was calculated by equation (3):

$$\% \text{ Degradation} = (C_0 - C_t)/C_0 \times 100 \quad (3)$$

J. Mex. Chem. Soc. **2025**, *69*(4)
Regular Issue
©2025, Sociedad Química de México
ISSN-e 2594-0317

The used Co_3O_4/CuO catalyst was collected, thoroughly washed with a mixture of H_2O and EtOH multiple times, and then dried for reuse in subsequent experiments. The results indicate that the catalytic activity remained consistent after four cycles for MO catalytic reduction. These findings demonstrate the stability and exceptional catalytic efficiency of the Co_3O_4/CuO nanocomposite in comparison to the fresh catalyst (Figures 7**(d)** and 8).

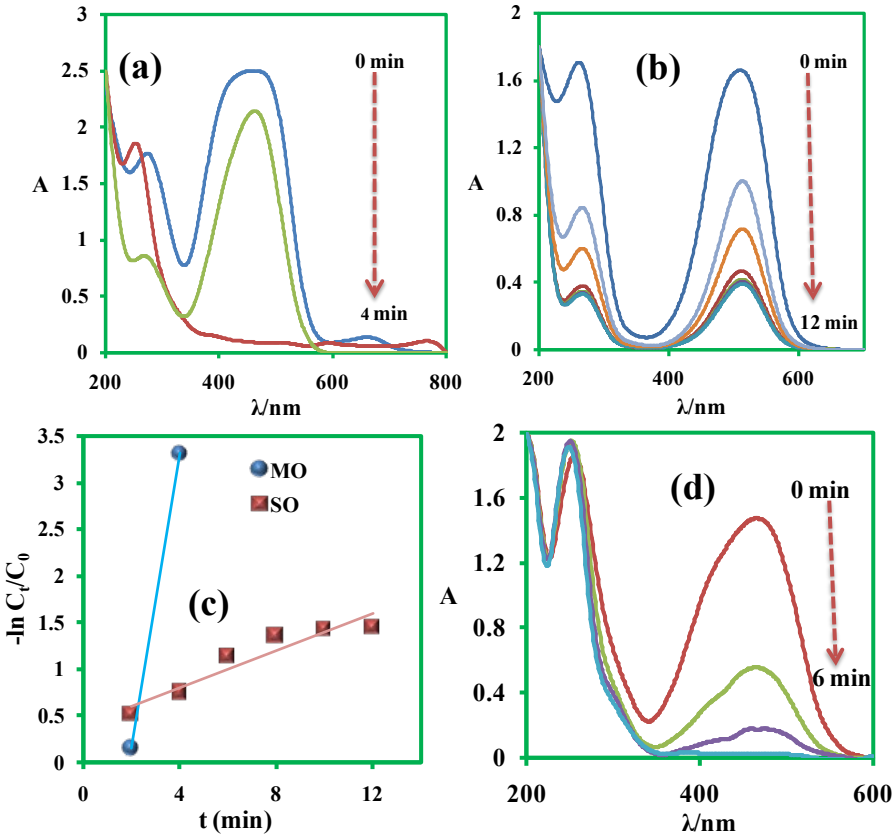

Fig.7. Degradation absorption spectra of MO **(a)** and SO **(b)** with $NaBH_4$ and Co_3O_4/CuO nanocomposite, **(c)** plot of $\ln(C_t/C_0)$ verses t (min) for Co_3O_4/CuO nanocomposite (3mg) (k=1.5 min^{-1} for MO and 0.1 min^{-1} for SO), **(d)** MO degradation with recycled catalyst.

Table 2. Comparative characteristics of catalysts for reducing methyl orange.

Entry	Catalyst	Amount	$NaBH_4$ conc.	Catalytic activity (%)	MO conc.	Time (min)	Ref.
1	$TiO_2/CoFe_2O_4/SiO_2$	5mg	20 mM	100 %	0.2 mM (k=0.59 min^{-1})	8	[38]
2	Ag@MIL-100(Fe)	1 mg	100mM	100 %	0.1 mM (k=0.236min^{-1})	5	[39]
3	BiTiOS	5 mg	13 mM	100 %	0.06 mM (k=0.809 min^{-1})	4	[40]
4	Co_3O_4/CuO	3 mg	20 mM	100 %	0.2 mM (k=1.5 min^{-1})	4	This work

J. Mex. Chem. Soc. **2025**, *69*(4)
Regular Issue
©2025, Sociedad Química de México
ISSN-e 2594-0317

Conclusions

The Co_3O_4/CuO nanocomposite was successfully synthesized using the calcination method, resulting in a hexagonal structure with an average particle size of approximately 25 nm. The combination of Co_3O_4 and CuO significantly enhanced the catalytic activity of the nanocomposite towards the reduction of 4-nitroaniline, 2-nitroaniline, and toxic dye pollutants (MO, SO). The synthesized Co_3O_4/CuO nanocomposite exhibits numerous merits, including excellent performance, ease of fabrication, cost-effectiveness, and recyclability, distinguishing it from other nanocatalysts. The results indicated that the reduction of 2-nitroaniline in the presence of Co_3O_4/CuO was superior to use CuO or Co_3O_4 alone, highlighting the synergistic effect between these metal oxides. Furthermore, the nanocatalyst maintained its activity after being recycled for four runs. This study provides a new strategy for developing an efficient reusable nanocatalyst for pollutant degradation via an environmentally safe process in which the nanocatalyst is easily collected from water thus mitigating its environmental impact.

Acknowledgments

We thank Biocomputational Laboratory, Department of Biology, Brawijaya University for provided the research facility for this study.

References

1. Lai, C.; Li, B.; Chen, M.; Zeng, G.; Huang, D.; Qin, L.; Liu, X.; Cheng, M.; Wan, J.; Du, C.; Huang, F.; Liu, S.; Yi, H. *Int. J. Hydrogen Energy.* **2018**, *43*, 1749-1757.
2. Bakhsh, E.M.; Ali, F.; Khan, S.B.; Marwani, H.M.; Danish, E.Y.; Asiri, A.M. *Int. J. Biol. Macromol*. **2019**, *131*, 666-675.
3. Ameen, F.; Dawoud, T.M.; Alshehrei, F.; Alsamhary, K.; Almansob, A. *Chemosphere.* **2021**, *271*, 129532.
4. de Barros, M.R.; Winiarski, J.P.; Elias, W.C.; de Campos, C.E.M.; Jost, C.L. *J. Environ. Chem. Eng*. **2021**, *9*, 105821.
5. Josephy, P.D.; Dhanoa, J.; Elzawy, G.; Heney, K.; Petrie, L.; Senis, C. *Environ. Mol. Mutagen.***2018**, *59*, 114-122.
6. Melinte, V.; Stroea, L.; Buruiana, T.; Chibac, A.L. *Eur. Polym. J.* **2019**, *121*, 109289.
7. Mei, X.; Ding, Y.; Wang, Y.; Yang, Y.; Xu, L.; Wang, Y.; Shen, W.; Zhang, Z.; Ma, M.; Guo, Z.; Xiao, Y.; Yang, X.; Zhou, B.; Xu, K.; Guo, W.; Wang, C. *Bioresour. Techno*l. **2020**, *307*, 123241.
8. Malakootian, M.; Gharaghani, M.A.; Dehdarirad, A.; Khatami, M.; Ahmadian, M.; Heidari, M.R.; Mahdizadeh, H. *J. Mol. Struct.* **2019**, *1176*, 766-776.
9. Amani, A.; Derikvand, Z.; Ghadermazi, M. *Inorg. Nano-Metal Chem.* **2025**, *55*, 864–879.
10. Pereira, I.D.S.; Bamberg, A.L.; Oliveira de Sousa, R.; Monteiro, A.B.; Martinazzo, R.; Posser Silveira, C.A.; de Oliveira Silveira, A. *J. Environ. Manag*. **2020**, *275*, 111203.
11. Smith, S.R. *Philos. Trans. A Math. Phys. Eng. Sci*. **2009**, *367*, 4005-4041.
12. Gu, Y.; Wang, Y.;; Zhang, H. *Spectrochim. Acta, Part A*. **2018**, *202*, 260-268.
13. Mazari, S.A.; Ali E.; Abro, R.; Khan, F.S.A.; Ahmed, I.; Ahmed, M.; Nizamuddin, S.; Siddiqui, T.H.; Hossain, N.; Mubarak, N.M.; Shah, A. *J. Environ. Chem. Eng,* **2021**, *9*, 105028.
14. (a) Gerent, G.G.; Santana, E.R.; Martins, E.C.; Spinelli, A. *Food Chem*. **2021**, *343*, 128419; (b) Azadbakht, A.; Abbasi, A.R.; Derikvand, Z.; Amraei S. *Mater. Sci. Engin.: C.* **2015**, *48*, 270-278; (c) Rahimi Fard, M.; Pourghobadi, Z. *Anal. Bioanal. Chem. Res*. **2018**, *5*, 249-259; (d) Saki, A.: Pourghobadi, Z.; Derikvand Z. *J. Electrochem Soc.* **2022**, *169*, 116507; (e) Alvandi, H.; Dorosti, N.; Afshar; F. *Mater. Tech*. **2022**, 37, 1691-1702.

J. Mex. Chem. Soc. **2025**, *69*(4)
Regular Issue
©2025, Sociedad Química de México
ISSN-e 2594-0317

15. (a) Santana, E.R.; de Lima, C.A.; Piovesan, J.V.; Spinelli, A. *Sens. Actuators B Chem.* **2017**, *240*, 487-496; (b) Beiranvand, S.; Abbasi, A.R.; Roushani, M.; Derikvand, Z.; Azadbakht, A. *J. Electroanal. Chem.* **2016**, *776*, 170-179; (c) Azadbakht, A.; Abbasi, A.R.; Derikvand, Z.; Karimi Z. Nano-Micro Lett. **2015**, *l.7*, 152-164; (d) Dorosti, N.; Delfan, B.; Khodadadi, M. *Appl. Organomet. Chem*. **2017**, *31*, e3875.
16. Maiyalagan,T.; Wang, X.; Manthiram, A. *RSC Ad*v. **2014**, *4*, 4028-4033.
17. Hosseinkhani, B.; Søbjer, L.S. g.; Rotaru, A.E.; Emtiazi, G., krydstrup, T. S.; Meyer, R.L. *Biotechnol. Bioeng.,* **2012**, *109*, 45-52.
18. Ai, L.; Li, L. *Chem. Eng. J.*, **2013**, *223*, 688-695.
19. Zhang, H.; Jiang, M.; Zhang, D.; Xia, Q. *Chem. Eng. Commun*. **2009**, *197*, 377-386.
20. Jiang, P.; Zhou, J.; Zhang, A.; Zhong, Y. *J. Environ. Sci.* **2010**, *22*, 500-506.
21. Kumar Dutta, R.; Verma S. *J. Environ. Chem.Eng.* **2017**, *5*, 4776-4787.
22. Liu, Z.; Yang, C.; Qiao, C. *FEMS Microbiol. Lett.*, **2007**, *277*, 150-156.
23. Modirshahla, N.; Behnajady, M.; Mohammadi-Aghdam S. *J. Hazard. Mater*. **2008**, *154*, 778-786.
24. Elfiad, A.; Galli, F.; Boukhobza, L.M.; Djadoun, A.; Boffito D.C. *J. Environ. Chem. Eng.* **2020**, *8*, 104214.
25. Ghosh, B.K.; Ghosh, N.N. *J. Nanosci. Nanotechnol.* **2018**, *18*, 3735-3758.
26. Wang, C.; Zhang, H.; Feng, Gao.; Shang, C. S.; Wang N. Z. *Catal. Commun.* **2015**, *72*, 29-32.
27. Tokazhanov, G.; Ramazanova, E.; Hamid, S.; Bae, S.; Lee W. *Chem. Eng. J.*, **2020**, *384*, 123252.
28. Wunder, S.; Polzer, F.; Lu, Y.; Mei, Y. *J. Phys. Chem. C*. **2010**, *114*, 8814-8820.
29. Derikvand, Z.; Rahmati, F.; Azadbakht, A. *Appl. Organomet. Chem.* **2019**, *33*, e4864.
30. Derikvand, Z.; Azadbakht, A.; Amiri Rudbari H. *J. Inorg. Organomet. Poly. Mater.* **2019**, *29*, 502-516.
31. Bahrami, M.; Derikvand, Z. *J. Mol. Struct.*, **2022**, *1254*, 132367.
32. Lellis, B.; F´avaro-Polonio, C.Z.; Pamphile, J.A.; Polonio, J.C. *Biotechnol. Res. Innov.,* **2019**, *3*, 275–290.
33. Burakov, A.E.; Galunin, E.V.; Burakova, I.V.; Kucherova, A.E.; Agarwal, S.; Tkachev, A. G.; Gupta, V.K. *Ecotoxicol. Environ. Saf*. **2018**, *148*, 702–712.
34. Alsukaibi, A.K.D. *Processes* **2022**, *10*, 1968.
35. Javaid, R.; Qazi, U.Y. *Int. J. Environ. Res. Public Health.* **2019**, *16*, 2066.
36. Hosseini, S. A. *Iran. J. Chem. Engin*. **2017**, *14*, 83-90.
37. Kumar, R.; Kumar, K.; Thakur, N. *Hybrid Advances*, **2024**, *5*, 100129.
38. Ma, J.; Deng , H.; Zhang , Z.; Zhang , L.; Qin, Z.; Zhang, Y.; Gao, L.; Jiao, T. *Colloids Surf. A: Physicochem. Eng. Asp*, **2022**, *632*, 127774.
39. Yin, J. J.; Ge, B. C.; Jiao, T. F.; Qin, Z. H.; Yu, M. Q.; Zhang, L. X.; Zhang, Q. R.; Peng Q. M. *Langmuir*, **2021**, *37*, 1267-1278.
40. Jeon, S.; Ko, J.W.; Bae, K.W. *Elastom. Compos*., **2020**, *55*, 191-198.
41. Lin, X.; Huang, T.; Huang, F.; Wang, W.; Shi, J. *J. Mater. Chem*. **2007**, *17*, 2145-2150.
42. Zarbakhsh, E.; Derikvand, Z. *Appl. Organomet. Chem.* **2024**, *38*, e7674.
43. Rattanakit, P.; Chutimasakul, T.; Darakai, V.; Nurerk, P.; Putnin, T. *S. Afr. J. Chem. Eng.* **2024**, *47*, 270–278.
44. Su, Z.; Wu, B.; Chen, L.; Tadesse Mosisa, M.; Zhang, P.; Wu, Q.; Kuo, D.-H.; Lu, D.; Ahmed Zelekew, O.; Lin, J.; Chen, X. *J. Sci.: Adv. Mater. Devices* **2023**, *8*, 100645.
45. Derikvand, Z.; Akbari, S.; Kouchakzadeh, G.; Azadbakht, A.; Nemati, A. *Russ. J. Phys. Chem. A.* **2019**, *93*, 2604-2612.
46. Arul, V.; M.G. Sethuraman, *Opt. Mater*. **2018**, *78*, 181-190.
47. Mallick, K.; Witcomb, M. Scurrell, M. *Mate. Chem. Phys*. **2006**, *97*, 283-287.